Acta Mech 229, 4101–4111 (2018)
https://doi.org/10.1007/s00707-018-2215-2

ORIGINAL PAPER

Davood Ghorbannia · Afshin Eghbalzadeh

Numerical study of the effect of length change on the flow pattern around a side weir in a converging channel

Received: 1 February 2018 / Revised: 28 May 2018 / Published online: 27 July 2018

Abstract Side weirs are among hydraulic structures which are utilized in flood control, urban sewage disposal networks, irrigation, and drainage channels. Today, thanks to computer science advancement, the use of numerical models has been increased owing to lesser time and lower costs compared with experimental models. The present study deals with investigating the flow pattern on a side weir in a converging rectangular channel using a commercial software employing RNG turbulence model and VOF method to simulate turbulence and free surface, respectively. One of the advantages of using side weirs is that after drainage it is unnecessary to continue the downstream channel with the previous width, and consequently it will be cost-effective. Comparing longitudinal velocities, water surface profiles, and flow discharge over a side weir with experimental results indicated the capability of the numerical model to simulate the flow pattern over a side weir. The effects of length changes of the side weir on the flow characteristics also were studied. Comparing parameters in different sections at the middle of the side weir showed that decreasing the length of the side weir increases the longitudinal velocity. Also, by decreasing the side weir length the passing discharge declined, and the free surface profile formed in higher height as well. The discrepancy between the specific energy at the upstream and that of the downstream of the weir for different side weir lengths was negligible.

Notations

A_x	Fractional area of the element in x-direction
A_y	Fractional area of the element in y-direction
A_z	Fractional area of the element in z-direction
F	Fluid volume fraction
f_i	Reynolds tensions in I direction
g_i	Gravity acceleration in I direction
u	Velocity component in x-direction
v	Velocity component in y-direction
w	Velocity component in z-direction
V_{F}	The ratio of fractional volume in each element
VOF	Volume of fluid
P	Pressure
L	The crest length of the side weir

D. Ghorbannia · A. Eghbalzadeh (✉)
Department of Civil Engineering, Razi University, Kermanshah, Iran
E-mail: eghbalzadeh@gmail.com

D. Ghorbannia
E-mail: davood.gh.1998@gmail.com

W	The crest height of the side weir
S	The crest thickness of the side weir
Q_0	Output discharge
Q_d	Outflow discharge
h_0	Output head
h_d	Outflow head
F_0	Output Froude number
F_d	Outflow Froude number
ρ	Fluid density

1 Introduction

A side weir is one of the most viable flow deviation structures which are constructed in the side wall of the main channel, and when the flow surface is higher than the spillway crest, some part of water drains to the outside of the channel. Overall, the flow over the side weirs is known as spatial variable, and the analytic solution of the governing equations of them is complicated. Hence, many experimental researches to investigate the flow properties over the side weirs have been fulfilled so far. By assuming this fact that the total energy is constant in the side weir in the main channel, De Marchi [1] presented an equation for spatial variable flow by decreasing discharge in the rectangular horizontal channel, irrespective of friction. He also introduced the flow discharge coefficient C_d to calculate the discharge flow of the side weir. Subramanya et al. [2] fulfilled studies about the flow discharge coefficient over side weirs in supercritical and subcritical conditions. They illustrated that the flow drop at the beginning of the side weir is insignificant. By measuring the velocity profile, they came to the conclusion that a side weir has a significant impact on the velocity distribution around the spillway. Ranga Raju et al. [3] presented an equation for calculating the discharge coefficient of the sharp crest and broad-crested side weir. Heger [4] studied the effect of flow depth, upstream velocity, output angle of the flow, and channel shape. He calculated the passing discharge over the side weir using correction coefficients. Singh et al. [5] manifested that in addition to upstream Froude number, the discharge coefficient depends on both weir's height and upstream depth. Borghei et al. [6] experimentally dealt with the effect of hydraulic and geometric parameters including upstream Froude number, the proportion of the weir's height to the upstream depth, and also the proportion of the side weir length to main channel width on the discharge coefficient which had been presented by De Marchi. Dourga and Pilai [7] conducted a study about a broad-crested weir under the supercritical condition. They concluded that the longitudinal component of the velocity vector passing over the weir is larger than the average velocity at the main channel. Emiroglu et al. [8] experimentally studied the flow over the labyrinth side weirs. They evaluated the effects of the hydraulic condition of the flow, weir geometry, and different dimensionless parameters on the flow discharge coefficient, flow surface profile, and velocity profile. Mohammed et al. [9] investigated the discharge coefficient equation for a side weir equipped with a steep crest. They considered few slopes for the crest in two opposite directions and the same direction of water movement through which by using experimental results and effective parameters the equations related to the discharge coefficient were obtained. Bagheri et al. [10] examined different components of velocity distribution and outflow discharge of the side weir. They concluded that at the end of the side weir a stagnation region has occurred and the change of side weir length in comparison with upstream Froude number has a larger influence on the outflow discharge. Michelazzo et al. [11] dealt with the investigation of the flow structure on the side weir with zero crest height with the aim of accurately calculating flow surface values, discharge, and velocity field in the main channel. Ameri et al. [12] discussed the initial discharge coefficient of a triangular–rectangular sharp-crested weir under subcritical condition. They presented precise equations of initial discharge coefficient for these types of weirs. Zahiri et al. [13] investigated the flow discharge over compound sharp-crested side weirs so that they were able to present a new method to predict flow discharge. Also, some numerical researches have studied the flow around side weirs. Among these researches, Qu [14] studied the flow pattern over a side weir employing a turbulence model and modeling the free surface using VOF method. He compared his model with the experimental data conducted by Subramanya et al. [2] and concluded that the stagnation region forms near the downstream edge of the side weir. Mangarulkar [15] dealt with the numerical simulation of the free surface of the side weir equipped with zero-height crest employing ANSYS ICEM software and compared the location of the stationary point obtained by analytic investigation with the results of numerical simulation. Aydin [16] simulated the flow field over a triangular labyrinth side weir with different turbulence models. He concluded that the RSM turbulence model compared with other turbulence models simulates fluctuations over

a labyrinth side weir with higher precision. Abdollahi et al. [17] dealt with numerical modeling of the flow field around triangular side weirs equipped with guide vanes using OpenFOAM and $k-\varepsilon$ turbulence model.

In all of the aforementioned researches, the main channel was prismatic. Maranzoni et al. [18] experimentally studied the flow over a side weir in a converging main channel. They came to the conclusion that a side weir in a converging channel in comparison with the prismatic channel can experience higher outflow efficiency. In addition, by deviating flow from the side weir, the flow discharge decrease in downstream and, hence, continuing channel with the previous width is unjustified. With respect to this fact that experimental researches are time-consuming and costly, numerical simulation appears to be an appropriate alternative to investigate the flow characteristics. The review of conducted researches indicates that the flow pattern around a side weir in a converging channel has not been studied so far. In this study, the numerical simulation of the flow passing over a side weir in a converging channel was done using a commercial software. After verification of the numerical results with experimental data, the effect of length change of the side weir on the outflow discharge and some other flow characteristics along the main channel were studied.

2 Governing equations

As mentioned, the numerical simulation of flow characteristics around a side weir was implemented using a commercial software. The continuity and Navier–Stokes equations were used as the governing equations on the flow. These equations are defined for an incompressible turbulent flow in non-dimensional, conservative form as:

$$\frac{\partial u_i^*}{\partial x_i^*} = 0, \tag{1}$$

$$\frac{\partial u_i^*}{\partial t^*} + \frac{\partial u_i^* u_j^*}{\partial x_i^*} = -\frac{\partial P^*}{\partial x_i^*} + \frac{1}{Re}\frac{\partial}{\partial x_j^*}\left((1+\nu_t^*)\left(\frac{\partial u_i^*}{\partial x_j^*} + \frac{\partial u_j^*}{\partial x_i^*}\right)\right) \tag{2}$$

where the variables are non-dimensionalized by the averaged velocity, U, and flow depth, H, at the inlet of the main channel. $u_i^* = \frac{u_i}{U}$ $(i = 1, 2, 3)$ are the non-dimensional Reynolds-averaged velocity components in x, y, and z directions, respectively. $x_i^* = \frac{x_i}{H}$ $(i = 1, 2, 3)$. $Re = \frac{UH}{\nu}$ is the Reynolds number, and $\nu_t^* = \frac{\nu_t}{\nu}$ is the non-dimensional turbulent viscosity. ν and ν_t are the molecular and turbulent viscosity, respectively. $P^* = \frac{P}{\rho U^2}$ is the non-dimensional modified pressure. ρ is the fluid density, and $t^* = \frac{t}{H/U}$ is the non-dimensional time.

In this study, the RNG-based $k-\varepsilon$ model was applied for the turbulence modeling. The turbulent viscosity is computed as follows:

$$\nu_t^* = C_\mu Re \frac{k^{*^2}}{\varepsilon^*}. \tag{3}$$

The non-dimensional transport equations of turbulent kinetic energy k and its rate of dissipation ε are given by:

$$\frac{\partial k^*}{\partial t^*} + \frac{\partial u_i^* k^*}{\partial x_i^*} = \frac{1}{Re}\frac{\partial}{\partial x_i^*}\left(\alpha_k \nu_{\text{eff}}^* \frac{\partial k^*}{\partial x_i^*}\right) + G^* - \varepsilon^*, \tag{4}$$

$$\frac{\partial \varepsilon^*}{\partial t^*} + \frac{\partial u_i^* \varepsilon^*}{\partial x_i^*} = \frac{1}{Re}\frac{\partial}{\partial x_i^*}\left(\alpha_\varepsilon \nu_{\text{eff}}^* \frac{\partial \varepsilon^*}{\partial x_i^*}\right) + C_{1\varepsilon}\frac{\varepsilon^*}{k^*}G^* - C_{2\varepsilon}\frac{\varepsilon^{*^2}}{k^*} - R^* \tag{5}$$

where

$$R^* = \frac{C_\mu \eta^3 \left(1 - \frac{\eta}{\eta_\circ}\right)}{\left(1 + C_3\eta^3\right)}\frac{\varepsilon^{*^2}}{k^*}, \tag{6}$$

$$\eta = \sqrt{\left(\frac{\partial u_i^*}{\partial x_j^*} + \frac{\partial u_j^*}{\partial x_i^*}\right)\frac{\partial u_i^*}{\partial x_j^*}}\frac{k}{\varepsilon}. \tag{7}$$

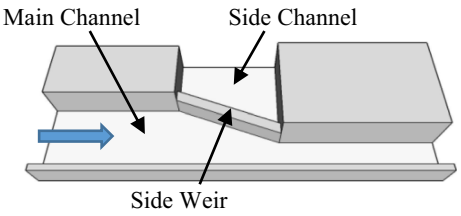

Fig. 1 Three-dimensional scheme of the computational domain

G is the production term of the turbulent kinetic energy:

$$G = \frac{\nu_t^*}{Re}\left(\frac{\partial u_i^*}{\partial x_j^*} + \frac{\partial u_j^*}{\partial x_i^*}\right)\frac{\partial u_i^*}{\partial x_j^*}. \tag{8}$$

$\nu_{\text{eff}}^* = \frac{\nu_{\text{eff}}}{\nu}$ is non-dimensional effective viscosity in which $\nu_{\text{eff}} = \nu_t\left(1 + \sqrt{\frac{C_\mu}{\nu}}\frac{k}{\sqrt{\varepsilon}}\right)^2$. $k^* = \frac{k}{U^2}$ and $\varepsilon^* = \frac{\varepsilon}{U^3/H}$ are the non-dimensional turbulent kinetic energy k and its dissipation rate ε, respectively. The quantities α_k and $\alpha_\varepsilon$are inverse Prandtl numbers for k and ε transport, respectively. C_μ, $C_{1\varepsilon}$, $C_{2\varepsilon}$, $\eta_\circ$, and C_3 are the constants of the turbulence model. The values of these constants are specified as:

$$C_\mu = 0.085, \quad C_{1\varepsilon} = 1.42, \quad C_{2\varepsilon} = 1.68, \quad \alpha_k = 1.39, \quad \alpha_\varepsilon = 1.39. \tag{9}$$

To simulate the free surface, VOF method was used. In this method, there is a variable known as fractional volume, F. The non-dimensional equation for the calculation of F in the three-dimensional state is defined as [16]:

$$\frac{\partial F}{\partial t^*} + u_i^*\frac{\partial F}{\partial x_i^*} = 0. \tag{10}$$

In the cells in which their volumes completely fill with water, the value of F is 1. In the cells in which $F = 0$, the whole volume of the cell is filled with air. Also, when $0 < F < 1$ a percentage of the cell is occupied by air and the remaining part is filled with water. Therefore, the free surface is obtained by determining a water surface in the surface cells of the flow on the basis of the fractional volume.

3 Verification of the numerical model

3.1 The computational domain characteristics

In this study, in order to verify the simulated model, the experimental results obtained by Maranzoni et al. [18] were used. The computational domain consists of a rectangular main channel without slope in which its length is 5.5 m and a side channel with the length 0.43 m (Fig. 1).

The width of the main channel upstream and downstream of the side weir is $B = 0.36$ m and $b = 0.18$ m, respectively (Fig. 2a). The beginning of the side weir is located at 1.95 m from the inlet of the main channel. The side weir length, L, along the main channel is 1.49 m. Also, its thickness, s, and height (W) are 5.5 cm and 18.3 cm, respectively (Fig. 2c). The discharge values Q, the flow depth (h), and the Froude number (F) were presented by Maranzoni et al. [18] at the beginning and end cross sections adjacent to the side weir (Fig. 2b). In this paper, the experimental case N15 with discharge 21.71 L/s and flow depth 0.214 m was used to verify the obtained results of the numerical simulation in comparison with the experimental ones.

3.2 Boundary condition and meshing

The boundaries of the computational domain shown in Fig. 1 are the inlet and outlet boundaries of the main channel, the outlet boundary of the side channel, solid walls, and the upper surface. At the inlet boundary,

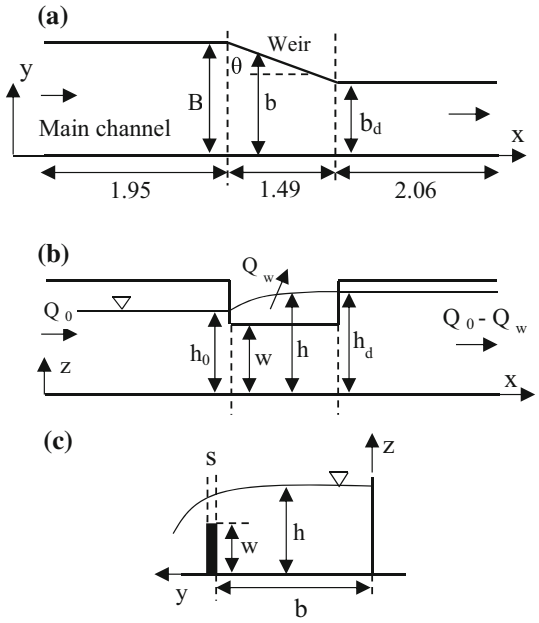

Fig. 2 Geometry and properties of the side weir in the converging channel. **a** plan, **b** side view, **c** cross section

known quantities are considered for velocity components while turbulent kinetic energy k and its dissipation rate ε are estimated using the relations as:

$$k_{\text{in}} = (0.1U)^2 \text{ and } \varepsilon_{\text{in}} = 10\, k_{\text{in}}^{3/2} C_{\mu}^{3/4}/(\kappa H) \tag{11}$$

where k_{in} and ε_{in} are turbulent kinetic energy and dissipation rate at the inlet, respectively.

At the outlet boundaries, gradients of all variables normal to the outlet boundary are set equal to zero. For the solid wall boundaries, a wall function approach is applied to avoid using a very fine mesh in the viscous sub-layer. Thus, the first grid near the wall is located in the logarithmic layer for which $y^+ > 11.6$. $y^+ = u_* y_1/\nu$ in which u_* is the shear velocity and y_1 is the distance of the first grid from the wall. In this first grid, the values of k and $\varepsilon$are computed as:

$$k_1 = u_*^2/C_{\mu}^{1/2} \text{ and } \varepsilon_1 = u_*^3/(\kappa y_1). \tag{12}$$

Finally, the symmetry boundary condition is used for the upper surface.

Uniform structured meshes were considered in the computational domain in x, y, and z directions. First, in order to select meshing with an appropriate number of cells, few meshes were examined. To investigate the precision of the numerical model, an average percentage error (APE) was used as follows:

$$\text{APE} = \frac{100}{N} \sum_{i=1}^{N} \left| \frac{R_{\text{measured}} - R_{\text{simulated}}}{R_{\text{measured}}} \right| \tag{13}$$

where R_{measured} and $R_{\text{simulated}}$ are experimental and numerical results, and N is the number of compared data between experimental and numerical results.

In Table 1, the number of meshes and also the average percentage errors (APE) in five different meshes for outflow discharges in X, $Q_0 - Q_w$, and Y, Q_w directions are shown. With respect to the comparison among all errors shown in Table 1, model 4 is adopted for further studies.

Table 2 gives information about the number of used cells in the selected model and boundary condition.

3.3 Flow depth in the side weir domain

To verify the model, the flow depth was compared between numerical and experimental results in Sections 1 and 2 in Fig. 3, and also along two axes of the channel, one in the middle of the channel width (central axis) and another one near the side weir (axes 3 and 4).

Table 1 Average percentage errors for the simulated outflow discharges

Models	Number of meshes	Average percentage errors	
		$Q_0 - Q_w$	Q_w
1	408,200	24.39	9.03
2	814,968	13.37	5.26
3	1,527,988	3.01	0.9
4	2,084,030	2.48	1.5
5	2,754,200	0.6	0.06

Table 2 Meshing properties and boundary condition

Meshing		
	Number of the cells in X direction	533
	Number of the cells in y direction	85
	Number of the cells in z direction	46

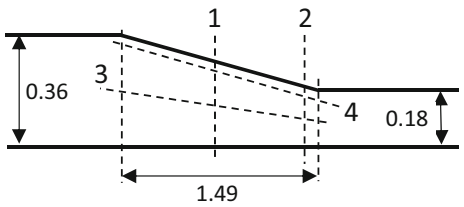

Fig. 3 The sections for comparing the flow depth in the side weir domain

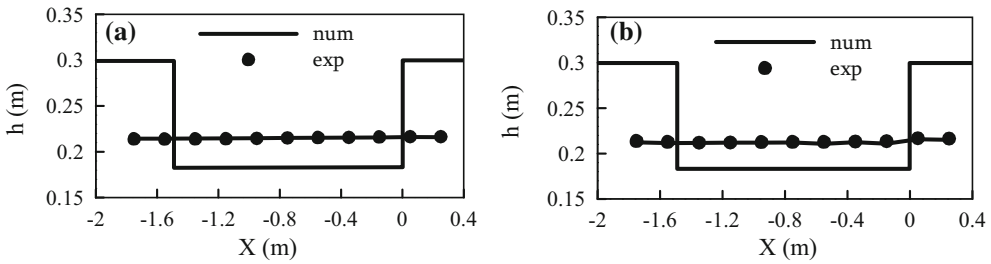

Fig. 4 Comparison of flow depth between experimental and numerical results. **a** section 3, **b** section 4

As can be seen in Figs. 4 and 5, there is an acceptable agreement between numerical and experimental results. The largest discrepancy on the weir occurred at the end of the weir where there is complicated flow condition (Fig. 5).

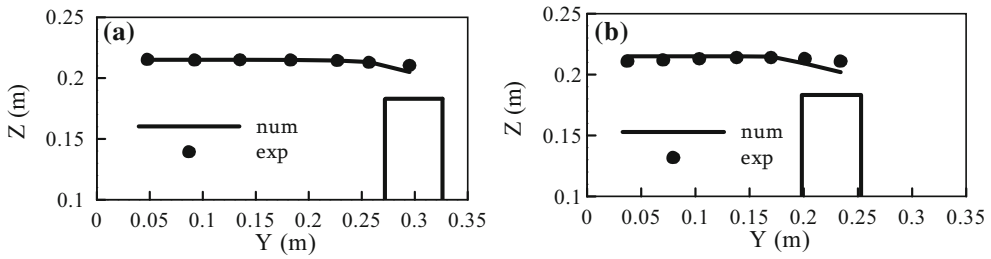

Fig. 5 Comparison of flow depth between experimental and numerical results in the cross sections. **a** 1, **b** 2

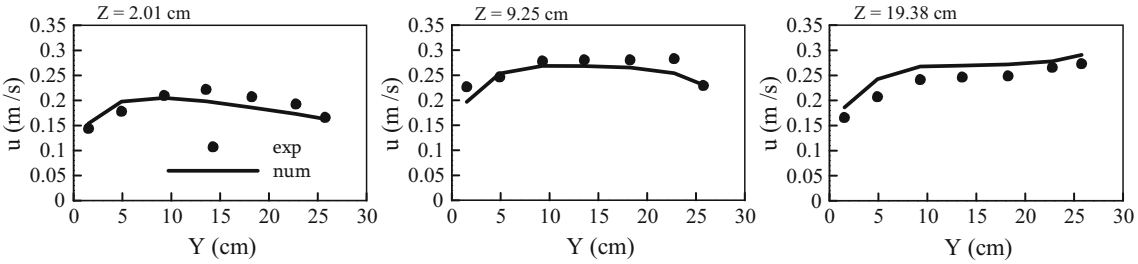

Fig. 6 Comparison of longitudinal velocity between experimental and numerical results in section 1

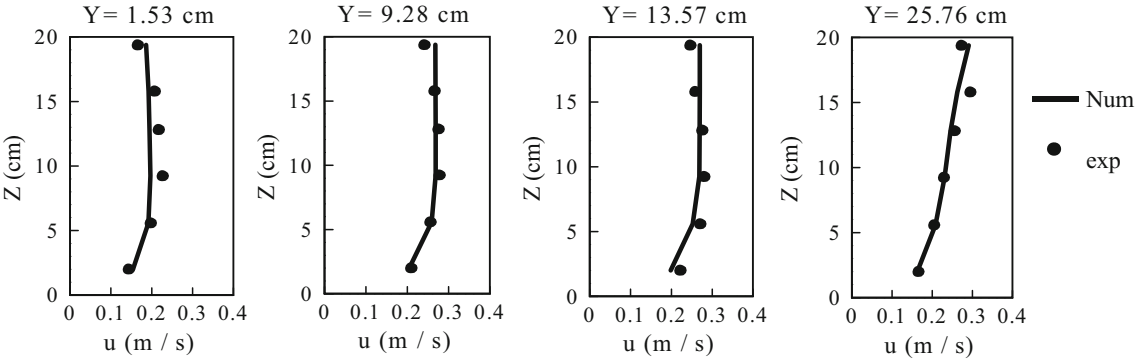

Fig. 7 Comparison of longitudinal velocity between experimental and numerical results in the vertical direction at different points in section 1

3.4 Comparison of velocity distribution in the different horizontal sections of the channel in the side weir domain

In Figs. 6 and 7, the longitudinal velocity values in section 1 (Fig. 3) are compared between numerical and experimental results. In Fig. 6, velocity values are manifested in different levels near the bed ($Z = 2.01$ cm), middle of the depth ($Z = 9.25$ cm), and near the water surface ($Z = 19.38$ cm) in the channel width. In Fig. 7 longitudinal velocity values in section 1 in the vertical direction and at different points are shown.

The average percentage error (APE) for the longitudinal velocity in Sect. 1 near the bed ($Z = 2.01$ cm) and flow surface ($Z = 19.38$ cm) is 7.64 and 9.92 %, respectively. This error value for the whole Sect. 1 is 6.25%. According to these results, it is concluded that the numerical model is able to simulate the flow around a side weir located in a converging rectangular channel with an acceptable accuracy.

4 Studying the effect of the length of the side weir on the flow characteristics

In the following the effect of the length of the side weir on the flow characteristics is studied. In Fig. 8, the four different lengths applied in this study are shown.

Figure 9 reveals the changes in discharge ratio (Q_w/Q_0 = the ratio of passing discharge over side weir to input discharge in the main channel) for different non-dimensional lengths (L/B) of the side weir. As can be seen in this Figure, by decreasing the length of the side weir less amount of flow deviates toward the side weir. Therefore, based on the obtained results, it is specified that the parameter of the side weir length plays a major role in passing discharge over the side weir. As seen in Fig. 9, the relation between Q_w/Q_0 and L/B is relatively linear.

In Figs. 10 and 11, longitudinal and transverse velocity distributions in Sect. 1 near the bed and flow surface are illustrated. As shown in Fig. 10, longitudinal velocities overall increase by declining the length of the side weir.

The transverse velocity values near the flow surface are significant near the edge of the side weir, and the values decrease toward the main channel wall (Fig. 11). Transverse velocity values increase by decreasing the length of the side weir and have the highest quantities near the water surface adjacent to the side weir where the flow passes it.

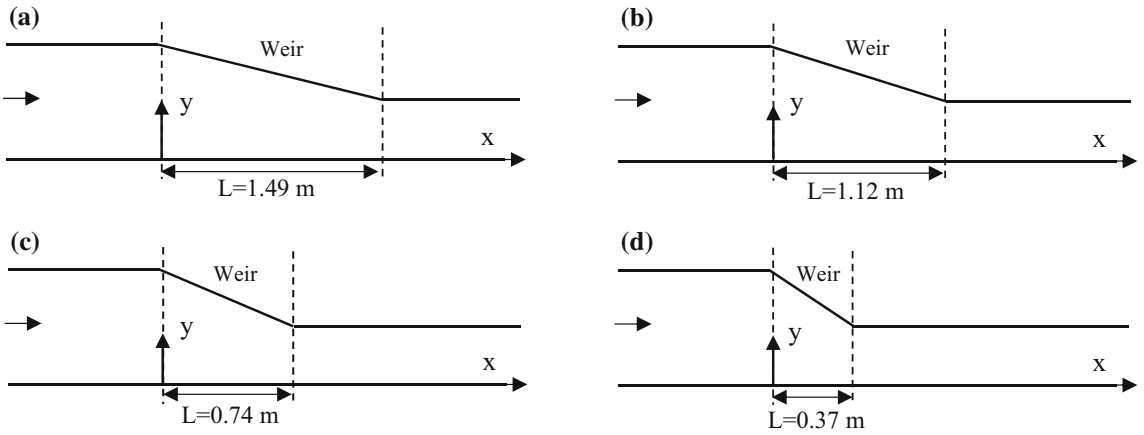

Fig. 8 The four different lengths of the side weir. **a** $L = 1.49$ m ($L/B = 4.14$), **b** $L = 1.12$ m ($L/B = 3.1$), **c** $L = 0.74$ m ($L/B = 2.07$), **d** $L = 0.37$ m ($L/B = 1.03$)

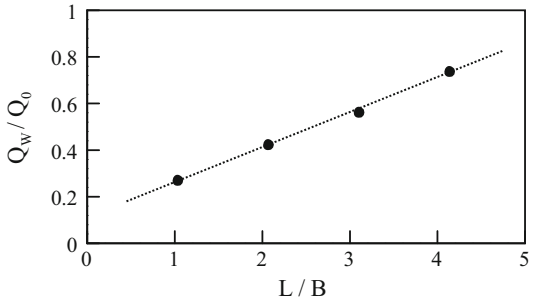

Fig. 9 Discharge ratio versus different lengths of the side weir

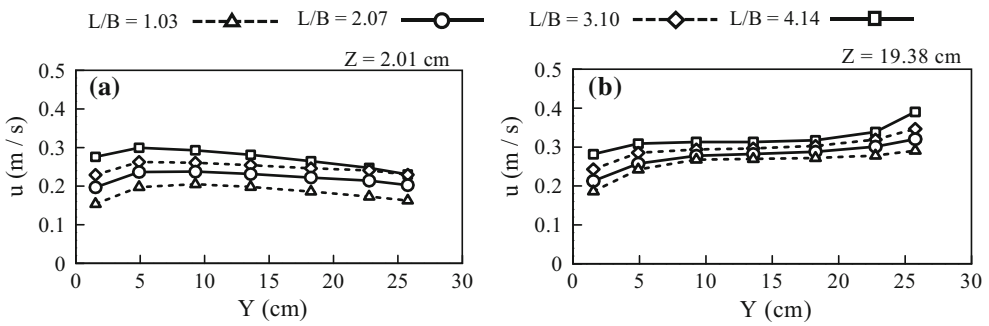

Fig. 10 Comparison of longitudinal velocity distribution in section 1, **a** near the channel bed ($Z = 2.01$ cm), **b** near the flow surface ($Z = 19.38$ cm)

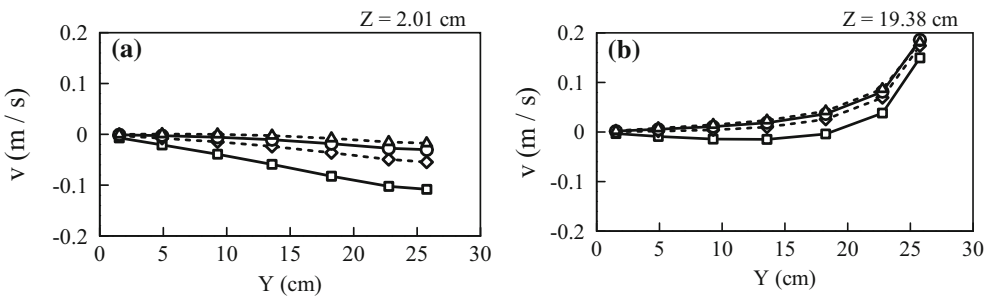

Fig. 11 Comparison of transverse velocity distribution in section 1. **a** $Z = 2.01$ cm, **b** $Z = 19.38$ cm

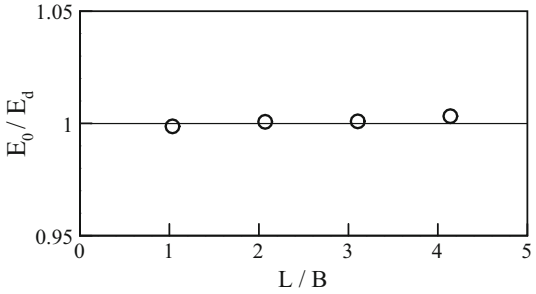

Fig. 12 The ratio of specific energy of the upstream to that of the downstream of the side weir versus different lengths

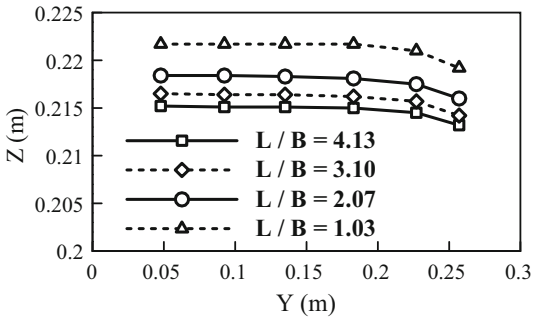

Fig. 13 Comparison of transverse flow surface profile in section 1 for different side weir lengths

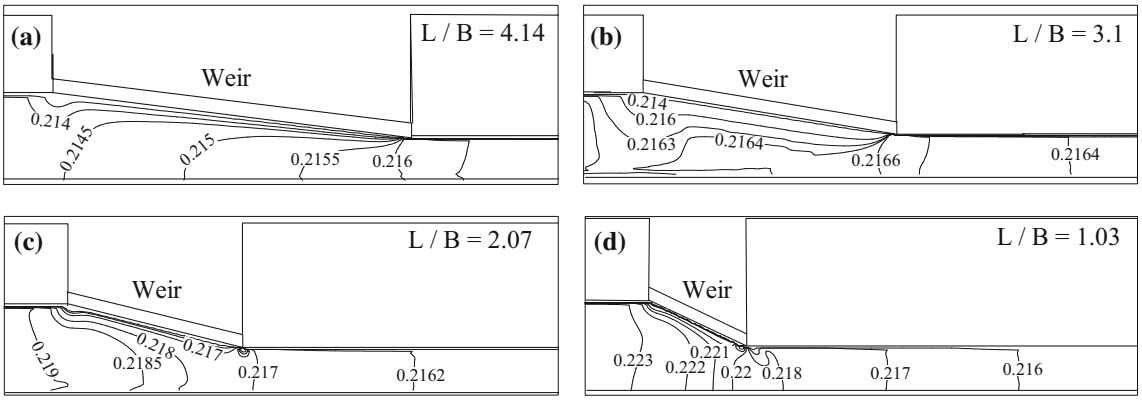

Fig. 14 Contour maps of the water surface in the side weir domain for various lengths of the weir. **a** $L/B = 4.14$, **b** $L/B = 3.1$, **c** $L/B = 2.07$, **d** $L/B = 1.03$

Figure 12 shows the ratio of the specific energy at the upstream to that of the downstream of the weir (E_0/E_d) versus the length changes of the side weir. With respect to Fig. 12, E_0/E_d for different lengths of the side weir remains relatively constant at the range 1. On the other hand, the length change effect on the specific energy along the side weir is negligible.

In Fig. 13, the transverse flow surface profile in Sect. 1 is compared for different lengths. As shown in this Figure, the flow depth increases by decreasing length of the side weir.

In Fig. 14, the contour line pattern of the water surface is illustrated in the side weir domain. As can be seen, the flow depth for two larger lengths increases and for two smaller lengths decreases along the side weir.

Figure 15 displays contour maps of longitudinal velocities at the water surface in the side weir domain. It can be seen that the longitudinal velocities for two larger lengths decrease and for two smaller lengths increase along the side weir.

Figure 16 gives information about the turbulent dynamic viscosity near the channel bed at $Z = 2.01$ cm. According to this Figure, it can be concluded that turbulent dynamic viscosity decreases with decreasing the length.

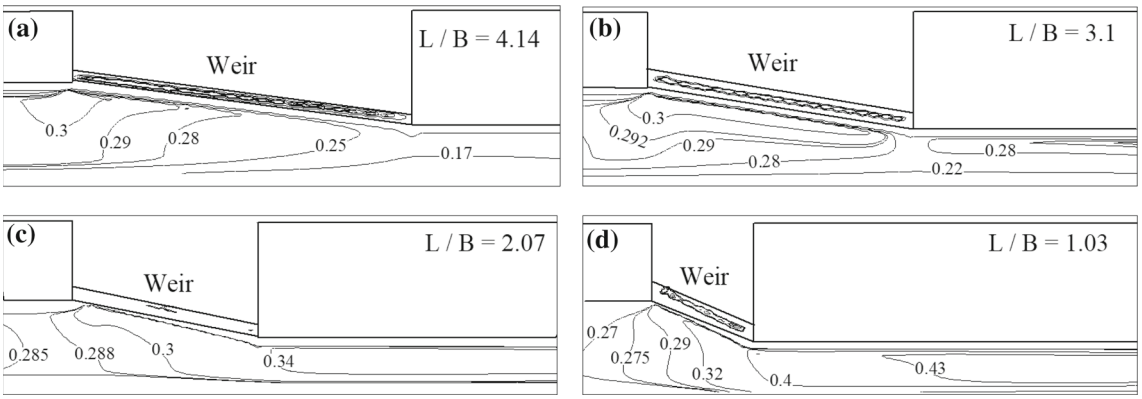

Fig. 15 Contour maps of the longitudinal velocities at the water surface in side weir domain for various lengths. **a** $L/B = 4.14$, **b** $L/B = 3.1$, **c** $L/B = 2.07$, **d** $L/B = 1.03$

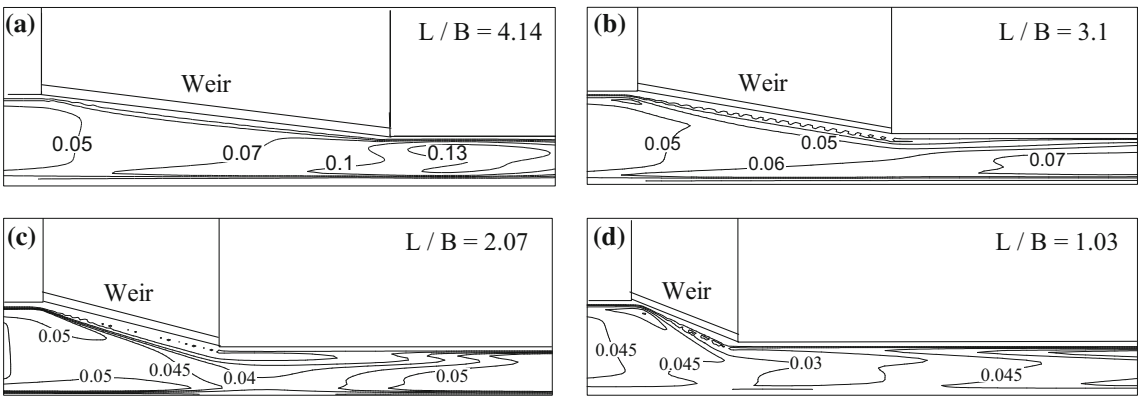

Fig. 16 Turbulent dynamic viscosity distribution near the channel bed for different lengths. **a** $L/B = 4.14$, **b** $L/B = 3.1$, **c** $L/B = 2.07$, **d** $L/B = 1.03$

5 Conclusions

In this paper, a numerical simulation of the flow pattern over a side weir in a converging rectangular channel was fulfilled using a commercial software. Comparing the numerical results of longitudinal velocities, the water surface profile and discharge over the side weir with experimental ones revealed that the results were in acceptable agreement. The results showed that decreasing the length of the side weir resulted in decreasing discharge over the side weir and also forming the water surface profile in higher height. Overall, by declining length of the side weir longitudinal and transverse velocities near the channel bed and water surface increase. The ratio of the specific energy at the upstream to that of the downstream of the weir for different lengths remained relatively constant. Finally, it was concluded that the turbulent dynamic viscosity decreased with decreasing the length.

References

1. De Marchi, G.: Essay on the performance of lateral weirs. L'Energ. Elettr. **11**, 849–860 (1934)
2. Subramanya, K., Awasthy, S.C.: Spatially varied flow over side-weirs. J. Hydraul. Div. **98**(1), 1–10 (1972)
3. Ranga Raju, K.G., Gupta, S.K., Prasad, B.: Side weir in rectangular channel. J. Hydraul. Div. **105**(5), 547–554 (1979)
4. Hager, W.H.: Lateral outflow over side weirs. J. Hydraul. Eng. **113**(4), 491–504 (1987)
5. Singh, R., Manivannan, D., Satyanarayana, T.: Discharge coefficient of rectangular side weirs. J. Irrig. Drain. Eng. **120**(4), 814–819 (1994)
6. Borghei, S.M., Jalili, M.R., Ghodsian, M.: Discharge coefficient for sharp-crested side weir in subcritical flow. J. Hydraul. Eng. **125**(10), 1051–1056 (1999)
7. Rao, K.D., Pillai, C.R.S.: Study of flow over side weirs under supercritical conditions. Water Resour. Manag. **22**(1), 131–143 (2008)

8. Emiroglu, M.E., Kaya, N., Agaccioglu, H.: Discharge capacity of labyrinth side weir located on a straight channel. J. Irrig. Drain. Eng. **136**(1), 37–46 (2009)
9. Mohammed, M.Y., Mohammed, A.Y.: Discharge coefficient for an inclined side weir crest using a constant energy approach. Flow Meas. Instrum. **22**(6), 495–499 (2011)
10. Bagheri, S., Heidarpour, M.: Characteristics of flow over rectangular sharp-crested side weirs. J. Irrig. Drain. Eng. **138**(6), 541–547 (2011)
11. Michelazzo, G., Oumeraci, H., Paris, E.: Laboratory study on 3D flow structures induced by zero-height side weir and implications for 1D modeling. J. Hydraul. Eng. **141**(10), 04015023 (2015)
12. Ameri, M., Dehghani, A.A., Ahmadi, A.: Elementary discharge coefficient of a triangular–rectangular sharp-crested side weir in subcritical flow. Int. J. River Basin Manag. **14**(1), 95–102 (2016)
13. Zahiri, A., Tang, X., Bagheri, S.: Flow discharge computation over compound sharp-crested side weirs. ISH J. Hydraul. Eng. **23**(3), 1–5 (2017)
14. Qu, J.: Three-dimensional turbulence modeling for free surface flows. Doctoral dissertation, Concordia University (2005)
15. Mangarulkar, K.: Experimental and numerical study of the characteristics of side weir flows. Doctoral dissertation, Concordia University (2010)
16. Aydin, M.C.: CFD simulation of free-surface flow over triangular labyrinth side weir. Adv. Eng. Softw. **45**(1), 159–166 (2012)
17. Abdollahi, A., Kabiri-Samani, A., Asghari, K., Atoof, H., Bagheri, S.: Numerical modeling of flow field around the labyrinth side-weirs in the presence of guide vanes. ISH J. Hydraul. Eng. **23**(1), 71–79 (2017)
18. Maranzoni, A., Pilotti, M., Tomirotti, M.: Experimental and numerical analysis of side weir flows in a converging channel. J. Hydraul. Eng. **143**(7), 04017009 (2017)